Differential Antigen Processing by Dendritic Cell Subsets in Vivo

Diana Dudziak *et al.*

Science **315**, 107 (2007);
DOI: 10.1126/science.1136080

tion. The *nfr1*, *nfr5*, *symrk*, and *ccamk* mutants are unable to form nodules in response to rhizobia inoculation. Thus, nodule formation on the *snf2* transgenic roots could not have resulted from contaminating rhizobia. In *nin* and *nsp2* mutants arrested before initiation of cell division induced by Nod-factor signaling, no spontaneous nodules were observed in *snf2* transgenic roots. Because *A. rhizogenes*–induced roots only develop when the hypocotyl wound site infection is used in lotus and because the *snf2* gene construct was integrated into the T-DNA, these results show that cytokinin signal perception acts upstream of cell division initiation (table S2). Furthermore, evidence for a central role of cytokinin and cytokinin perception downstream of Nod-factor signal transduction comes from the additive effect of *snf1-1* and *snf2* mutations. The *snf1-1* mutants synthesize a CCaMK protein impaired in autophosphorylation (*20*, *21*) and develop an average of 7 ± 0.9 (95% confidence interval) spontaneous nodules, whereas *snf2* mutants develop 3 ± 0.5. The *snf1-1 snf2* double mutants exceed both with 17 ± 0.9 spontaneous nodules. Parallel signaling cannot be excluded, but more likely, the deregulated signaling in *snf1* results in a local increase in cytokinin levels transcriptionally up-regulating *snf2* (Fig. 2D) and amplifying spontaneous nodulation. The previously reported expression of a *Nin*-GUS promoter fusion in *snf1* nodule primordia and the absence of epidermal expression in *snf1* roots (*20*) further suggest cytokinin signaling is a cortical response. Conversion of cortical cells into nodule stem cells or subsequent organ development seem therefore tightly controlled. We tested this in a hypernodulating *har1-1* mutant (*22*). Homozygous *snf2 har1-1* double mutants developed an average of 14 ± 1.4 spontaneous nodules, whereas *snf2* mutants developed an average of 3 ± 0.5, and *har1-1*, none (fig. S6). This indicates that only a few cells dedifferentiate or that only a few dedifferentiated cells sustain cell divisions during the *snf2* nodule-initiation process. The shoot controlled autoregulation of the root nodule number (*22*) is thus acting downstream of cytokinin signaling–induced activation of root nodule founder cells (Fig. 4C).

From *Arabidopsis* and tobacco, there is evidence for cytokinin regulation of cell cycle phase transitions (*23*) and for overlapping roles for three AHK receptors in maintaining stem cells and cell divisions during organ formation (*13*). Phytohormones have also been implicated in nodule organogenesis. Applications of auxin transport inhibitors resulted in empty nodule-like structures, which suggested that local inhibition of auxin transport (*24*) sensitizes cells for division. Other experiments showed that externally supplied cytokinin induces cortical cell division and activation of *Enod12*, *Enod40*, and *Enod2* genes (*4*, *25*), and expression of a cytokinin biosynthesis *tzs* gene in a nodulation-deficient *Sinorhizobium meliloti* resulted in nodule-like structures (*5*).

Here we show conclusively that cytokinin signaling plays an important role in plant meristem formation and is directly involved in initiating root nodule organogenesis. The opposite phenotype effects of the *snf2* gain-of-function and *hit1* loss-of-function mutations reported in the accompanying paper (*18*), together with the reduced nodulation observed after down-regulation of the corresponding gene in *Medicago* (*26*), clearly demonstrate that cytokinin signaling is necessary and sufficient for the dedifferentiation and cell proliferation leading to root nodule formation.

References and Notes

1. S. Radutoiu *et al.*, *Nature* **425**, 585 (2003).
2. E. B. Madsen *et al.*, *Nature* **425**, 637 (2003).
3. L. Tirichine, E. K. James, N. Sandal, J. Stougaard, *Mol. Plant Microbe Interact.* **19**, 373 (2006).
4. Y. Fang, A. M. Hirsch, *Plant Physiol.* **116**, 53 (1998).
5. J. B. Cooper, S. R. Long, *Plant Cell* **6**, 215 (1994).
6. J. Stougaard, D. Abildsten, K. A. Marcker, *Mol. Gen. Genet.* **207**, 251 (1987).
7. J. Hansen *et al.*, *Plant Cell Rep.* **8**, 12 (1989).
8. A. P. Mahonen *et al.*, *Genes Dev.* **14**, 2938 (2000).
9. T. Suzuki *et al.*, *Plant Cell Physiol.* **42**, 107 (2001).
10. T. Kakimoto, *Plant Cell Physiol.* **42**, 677 (2001).
11. V. Anantharaman, L. Aravind, *Trends Biochem. Sci.* **26**, 579 (2001).
12. J. Pas, M. von Grotthuss, L. S. Wyrwics, L. Rychlewski, J. Barciszewski, *FEBS Lett.* **576**, 287 (2004).
13. N. Nishimura *et al.*, *Plant Cell Physiol.* **45**, 1485 (2004).
14. C. E. Hutchison, J. J. Kieber, *Plant Cell* **14** (suppl.), S47 (2002).
15. D. P. Lohar *et al.*, *Plant J.* **38**, 203 (2004).
16. A. M. Rashotte, S. D. Carson, J. P. To, J. J. Kieber, *Plant Physiol.* **132**, 1998 (2003).
17. I. Hwang, J. Shen, *Nature* **413**, 383 (2001).
18. J. D. Murray *et al.*, *Science* **315**, 101 (2007); published online 16 November 2006 (10.1126/science.1132514).
19. S. Niwa *et al.*, *Mol. Plant Microbe Interact.* **14**, 848 (2001).
20. L. Tirichine *et al.*, *Nature* **441**, 1153 (2006).
21. C. Gleason *et al.*, *Nature* **441**, 1149 (2006).
22. L. Krusell *et al.*, *Nature* **420**, 422 (2002).
23. T. Kakimoto, *Annu. Rev. Plant Biol.* **54**, 605 (2003).
24. U. Mathesius *et al.*, *Plant J.* **14**, 23 (1998).
25. C. Dehio, F. J. de Bruijn, *Plant J.* **2**, 117 (1992).
26. S. Gonzalez-Rizzo, M. Crespi, F. Frugier, *Plant Cell* **18**, 2680 (2006).

27. L.T. was supported by the Lotus Training Network grant HPRN-CJ-2000-00086. *Lhk1* gene accession number: AM287032; *LHK1* mRNA accession number: AM287033.

Supporting Online Material

www.sciencemag.org/cgi/content/full/1132397/DC1
Materials and Methods
Figs. S1 to S7
Tables S1 and S2
References

12 July 2006; accepted 7 November 2006
Published online 16 November 2006;
10.1126/science.1132397
Include this information when citing this paper.

Differential Antigen Processing by Dendritic Cell Subsets in Vivo

Diana Dudziak,[1] Alice O. Kamphorst,[1] Gordon F. Heidkamp,[1] Veit R. Buchholz,[1] Christine Trumpfheller,[2] Sayuri Yamazaki,[2] Cheolho Cheong,[2] Kang Liu,[1] Han-Woong Lee,[3] Chae Gyu Park,[2] Ralph M. Steinman,[2] Michel C. Nussenzweig[1,4]*

Dendritic cells (DCs) process and present self and foreign antigens to induce tolerance or immunity. In vitro models suggest that induction of immunity is controlled by regulating the presentation of antigen, but little is known about how DCs control antigen presentation in vivo. To examine antigen processing and presentation in vivo, we specifically targeted antigens to two major subsets of DCs by using chimeric monoclonal antibodies. Unlike $CD8^+$ DCs that express the cell surface protein CD205, $CD8^-$ DCs, which are positive for the 33D1 antigen, are specialized for presentation on major histocompatibility complex (MHC) class II. This difference in antigen processing is intrinsic to the DC subsets and is associated with increased expression of proteins involved in MHC processing.

Lymphoid organ DCs are composed of distinct subsets (*1*–*5*). In the spleen, two major types of DCs are found: The first is positive for the CD8 marker and the C-type lectin CD205 ($CD8^+DEC205^+$), and the second lacks CD8 but expresses the antigen recognized by the 33D1 monoclonal antibody (mAb) $CD8^-33D1^+$. These subsets reside in different anatomic locations—$CD8^+DEC205^+$ DCs are in the T cell zone, whereas $CD8^-33D1^+$ DCs are in the red pulp and marginal zone—and the two can be further distinguished by a number of surface markers (*4*, *5*) (Fig. 1, A to C, and fig. S1).

$CD8^+DEC205^+$ DCs appear to be specialized for uptake of dying cells and play a unique role in resistance to certain viral infections (*6*–*8*). Notable among the other distinctions between the two cell types is the suggestion that $CD8^+DEC205^+$ DCs are specialized for cross-presentation, which is the ability to process nonreplicating antigens for presentation to T cells by class I molecules of the major histocompatibility complex (MHCI)

[1]Laboratory of Molecular Immunology, The Rockefeller University, New York, NY 10021, USA. [2]Laboratory of Cellular Immunology and Physiology, The Rockefeller University, New York, NY 10021, USA. [3]Department of Biochemistry, College of Sciences, Yonsei University, Seoul 120-749, Korea. [4]Howard Hughes Medical Institute, The Rockefeller University, New York, NY 10021 USA.

*To whom correspondence should be addressed. E-mail: nussen@rockefeller.edu

(*7*–*12*). However, a direct comparison of the capacity of the two subsets to process antigen in vivo has been lacking.

We identified the antigen recognized by the 33D1 mAb through a combination of gene array and candidate gene approaches and found it to be dendritic cell inhibitory receptor–2 (DCIR2) [Fig. 1, D and E; fig. S2 and (*13*)]. DCs are highly enriched in lectins, and in addition to DCIR2 and DEC205, the $CD8^+DEC205^+$ and $CD8^-33D1^+$ DCs differed in expression of a number of other lectins (Fig. 1D and fig. S2B). To evaluate regulation of antigen processing and T cell activation by the two DC subsets in vivo, we delivered antigens to each cell type in situ using chimeric αDEC205 (*14*) and 33D1 antibodies (*15*) [fig. S3 and (*13*)]. Delivery of ovalbumin (OVA) antigen by the injected antibodies was monitored after DC purification by antigen presentation in vitro to transgenic OT-I or OT-II T cells specific for OVA peptides presented on MHC class I or MHC class II, respectively (*14*, *16*). As previously reported, purified DCs targeted with αDEC205-OVA in vivo induced both OT-I and OT-II T cell proliferation in vitro, although the extent of OT-II proliferation was relatively modest (Fig. 1F) (*14*, *16*). In contrast, antigen delivered with the 33D1 antibody elicited high levels of OT-II but no detectable OT-I T cell responses (Fig. 1F). B cells and other non-DCs purified from mice injected with αDEC205-OVA or 33D1-OVA failed to present OVA either to OT-I or OT-II T cells (Fig. 1F). The specificity of targeting was made apparent by the specific localization of αDEC205 on $CD8^+DEC205^+$ DCs and 33D1 on $CD8^-33D1^+$ DCs after chimeric antibody injection in vivo (Fig. 1G). In addition, both antibodies were internalized by the cells, although the kinetics of 33D1 internalization was slower than for DEC205, and the amount of internalized αDEC205-OVA was greater than the amount of internalized 33D1-OVA (Fig. 1H and fig. S4). Neither antibody altered DC maturation status, as determined by surface expression of MHCII, CD40, CD69, CD80, and CD86 (fig. S5). Finally, the difference in presentation between the two DC subsets in vivo was not due to a difference in their ability to present peptides once processed, because the two were equivalent in presentation of antigen to the same transgenic T cells when processed peptides were added to in vitro cultures (fig. S6). We conclude that DCs targeted by αDEC205-OVA or 33D1-OVA in vivo are distinct in their ability to present antigen on MHCI and MHCII in vitro.

To examine T cell activation in response to antigen presentation in vivo, we labeled OT-I and OT-II T cells with 5-(6)-carboxyfluorescein diacetate succinimidyl diester (CFSE), a reporter dye for cell division, and monitored the cells after adoptive transfer to a new host (*13*). As observed in vitro, αDEC205-OVA induced MHC class I–restricted OT-I responses with greatest efficiency, whereas 33D1-OVA primarily elicited MHC class II–restricted OT-II responses

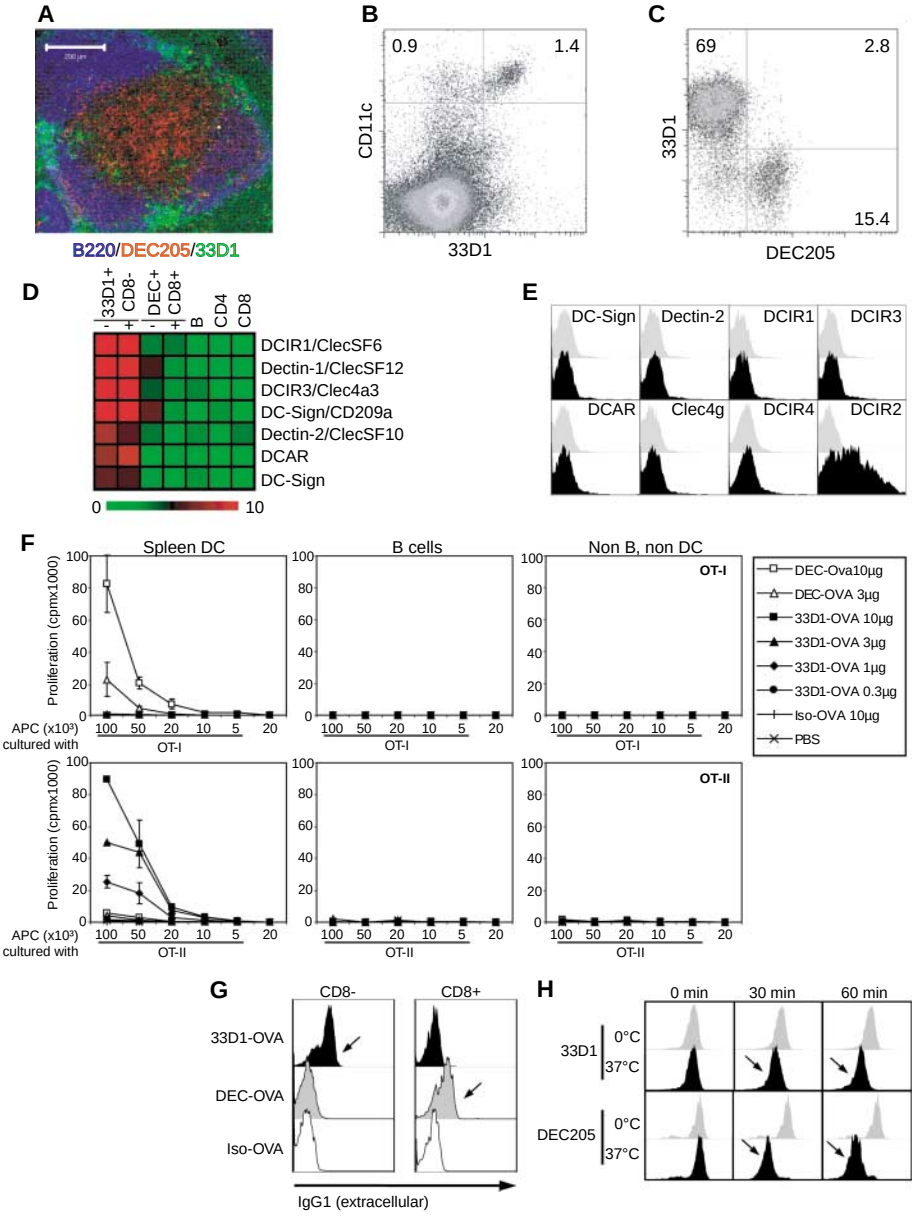

Fig. 1. CD4 and CD8 T cell responses to targeted antigen in vitro. (**A**) Micrograph shows immunohistochemistry of 33D1 (green), αDEC205 (red), and αB220 (blue). (**B** and **C**) Dot plots show splenocytes analyzed by flow cytometry for expression of CD11c and 33D1 (B) and 33D1 and DEC205 gated on $CD11c^{high}$ cells (C). Numbers indicate percentages of total splenocytes and $CD11c^+$ splenocytes, respectively. (**D**) Affymetrix gene array analysis of candidate C-type lectins. RNA was prepared from FACS-sorted B cells, $CD4^+$ T cells, $CD8^+$ T cells, $CD8^+DEC205^+$, and $CD8^-33D1^+$ WT (–) and Flt3L-melanoma (+) injected mice. Each bar represents a mean of three individual gene arrays. List of candidate genes showing difference between $CD8^+DEC205^+$ and $CD8^-33D1^+$ subsets in WT- and Flt3L-injected mice. (**E**) Histograms show 33D1-A647 (black) and isotype IgG2b-A647 antibody (gray) staining of 293T cells transiently transfected with the indicated cDNAs. (**F**) Graphs show [^{3}H]thymidine incorporation by 10^5 OT-I (upper panels) or OT-II T cells (lower panels) cultured with the indicated numbers of DCs, B cells, or non-B non-DCs purified from C57BL/6 mice injected with 10 μg of 33D1-OVA, αDEC-OVA, or Iso-OVA 12 hours earlier. (**G**) Histogram shows extracellular αDEC205 or 33D1 antibodies on $CD8^+DEC205^+$ and $CD8^-33D1^+$ DCs 30 min after intravenous injection of 10 μg of αDEC205-OVA, 33D1-OVA, or Iso-OVA control, visualized with anti-mouse IgG-FITC (fluorescein isothiocyanate). (**H**) Histograms show internalization of purified rat 33D1 (upper panels) or rat αDEC205 antibodies (lower panels) after incubation at 37°C for 0, 30, or 60 min (black), or cell surface expression after incubation on ice for a further 0, 30, or 60 min (gray). Cells were gated on $CD11c^+CD8^-$ and $CD11c^+CD8^+$ DCs.

(Fig. 2A). By in vivo dose-response experiments, comparing cell division and T cell expansion after transfer, 33D1-OVA was a factor of 10 less effective in presentation to OT-I T cells and 10 times as effective in presentation to OT-II T cells as αDEC205-OVA (Fig. 2, A and B). Antigen presentation after a single administration of either αDEC205-OVA (*16*) or 33D1-OVA was long-lasting (Fig. 2C). Thus, OT-I T cells proliferated in response to antigen even when they were transferred 10 days after αDEC205-OVA injection, and OT-II T cells proliferated when cells were transferred up to 5 days after 33D1-OVA injection (Fig. 2C). However, T cells proliferating in response to antigen delivered by targeting antibodies in the steady state were rapidly deleted, and the remaining cells were unresponsive to further stimulation in vitro (Fig. 2, D and E). In contrast, when antigen delivery by 33D1 was combined with DC activation by αCD40, the expanded T cell population persisted and demonstrated strong recall responses to antigen challenge in vitro (Fig. 2, F and G). Thus, antigen delivery to $CD8^{-}33D1^{+}$ DCs in vivo results in preferential MHCII-restricted antigen presentation. Nevertheless, delivery of antigens to both DC subsets in the steady state leads to T cell tolerance, whereas targeting in combination with DC maturation by CD40 ligation leads to expansion of T cell clones that remain responsive to antigen.

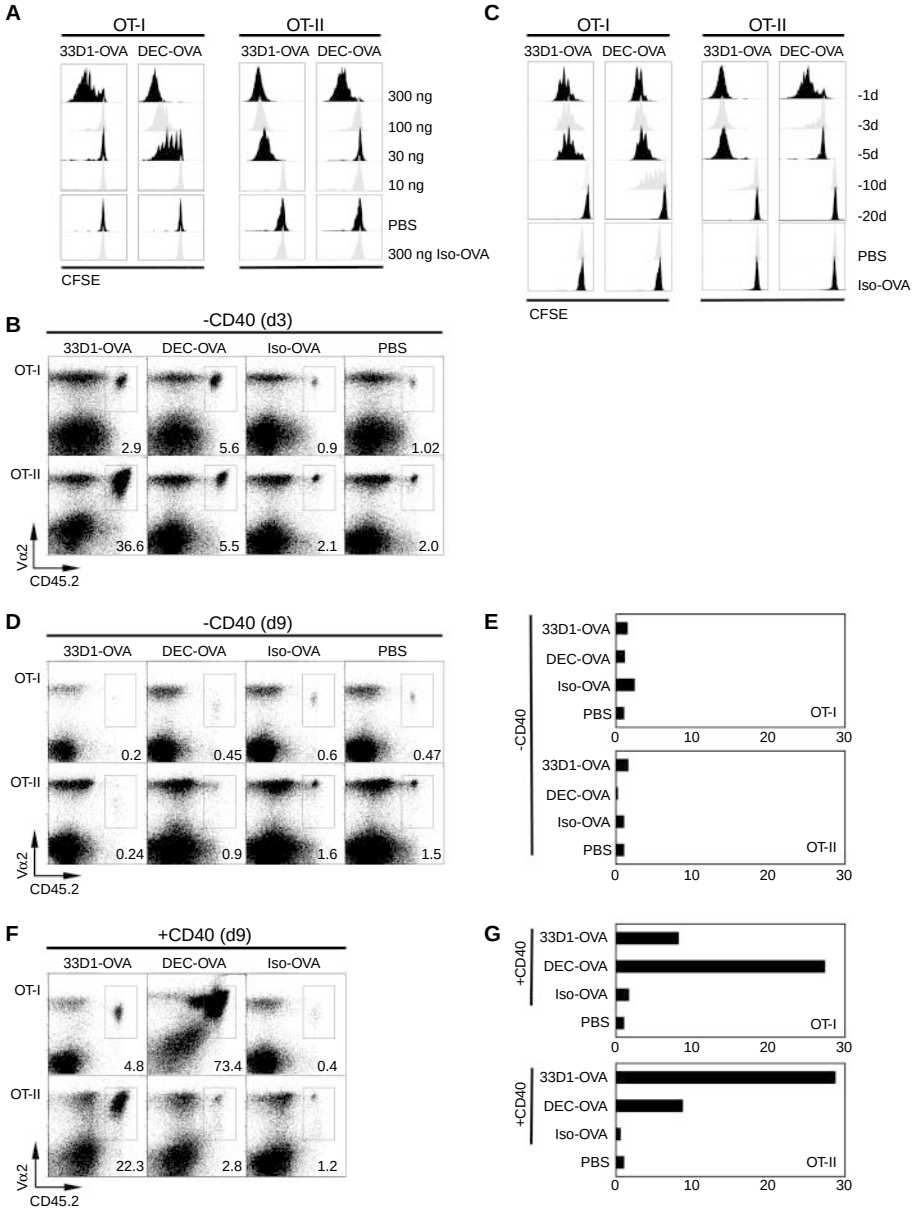

Fig. 2. CD4 and CD8 T cell responses to targeted antigen in vivo. (**A**) Histograms show proliferation as measured by CFSE dye dilution by OT-I (left) or OT-II (right) T cells 3 days after injection of varying amounts of 33D1-OVA, αDEC-OVA, or control antibodies. (**B**) Dot plots show the relative numbers of OT-I (upper panels) or OT-II (lower panels) T cells remaining in spleen 3 days after injection of 300 ng of 33D1-OVA, αDEC-OVA, or Iso-OVA. Numbers indicate percentages of gated $CD4^{+}$ or $CD8^{+}$ that were $Va2^{+}CD45.2^{+}$. (**C**) As in (A), but T cell transfer was performed 1, 3, 5, 10, or 20 days after injection of 3 μg of 33D1-OVA, αDEC-OVA, or Iso-OVA. (**D**) As in (B), but 9 days after injection of chimeric antibodies. (**E**) Bar graphs show $[^{3}H]$thymidine incorporation by CD4 or CD8 T cells purified on day 9 after injection of 3 μg of 33D1-OVA, αDEC-OVA, or Iso-OVA and challenged with antigen in vitro. (**F**) Same as (D), except that 50 μg of αCD40 antibody was injected with the targeting antibodies to induce DC maturation. (**G**) Same as (E), except that 50 μg of αCD40 antibody was injected with the targeting antibodies to induce DC maturation. Panels are representative of two to four independent experiments. PBS, phosphate-buffered saline.

To examine the mechanism responsible for differential antigen presentation by the two DC subsets, we assayed formation of MHCII hen egg lysozyme (HEL) peptide complexes (MHCII-p) by using a mAb specific for this complex (*17*). $CD8^{+}DEC205^{+}$ DCs showed small amounts of surface MHCII-p 3 hours after injection of αDEC205-HEL, but this was no longer visible after 1 day (Fig. 3A). In contrast, $CD8^{-}33D1^{+}$ DCs targeted with 33D1-HEL antibodies displayed much higher levels of MHCII-p after 3 hours and continued to display MHCII-p 2 days after targeting (Fig. 3A, arrows). MHCII-p formation was specific for the targeting antibody and independent of DC activation because mice deficient in the lipopolysaccharide (LPS) Toll-like receptor 4 (TLR-4) were indistinguishable from controls in this assay (Fig. 3, A and B) (*13*). We conclude that antigens delivered by the 33D1 antibody to $CD8^{-}33D1^{+}$ DCs in the steady state are processed and transferred to the cell surface as MHCII-p more efficiently than are antigens delivered by αDEC205 to $CD8^{+}DEC205^{+}$ DCs.

To determine whether the observed differences in antigen processing were due to cell-intrinsic differences between the two DC subsets, we produced transgenic mice that express human DEC205 (CD11c-hDEC205 B10.BR transgenic mice) on both DC subsets and performed targeting experiments with an αhDEC205 antibody that does not cross-react with mouse DEC205 (*18*) [fig. S7; note that CD11c-hDEC205 mice show position effect variegation and hDEC205 is equally expressed and variegated on both DC subsets (*13*)]. Both subsets were specifically targeted by αhDEC205-HEL in transgenic mice but not wild-type (WT) controls in vivo as measured by surface staining with antibodies to immunoglobulin G (anti-IgG) (fig. S8). However, only $CD8^{-}33D1^{+}$ CD11c-hDEC205 transgenic DCs showed high levels of MHCII-p after αhDEC205-HEL or MHCII-p presentation after αhDEC205-OVA injection (Fig. 3C and fig. S9). To further compare presentation by αDEC205-OVA and 33D1-OVA targeting in the same cell, we infected bone marrow–derived DCIR2-negative DCs with a retrovirus encoding DCIR2

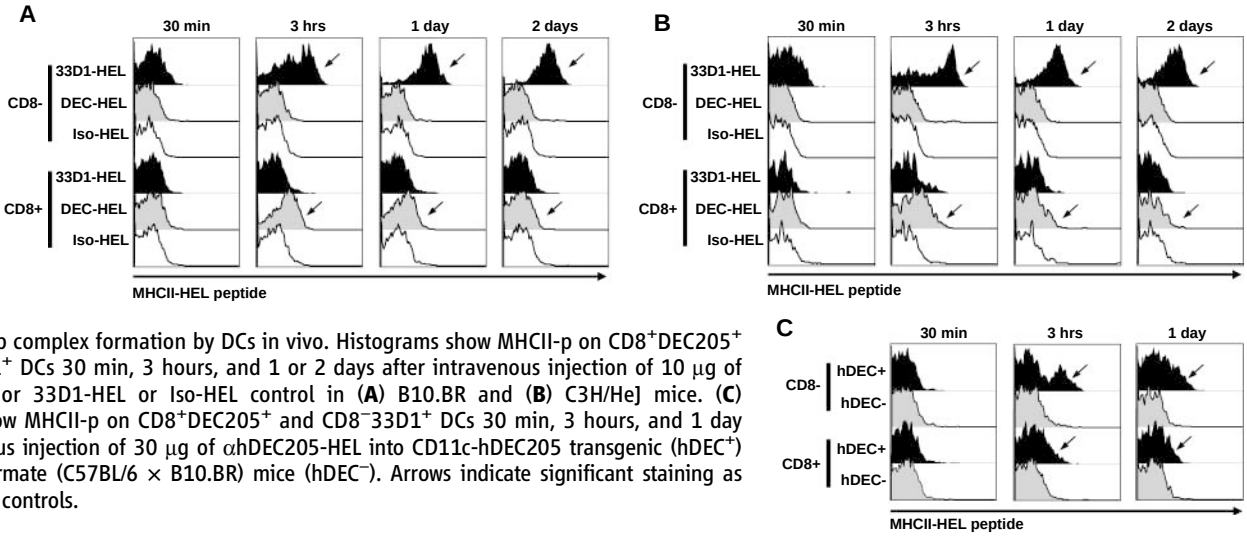

Fig. 3. MHCII-p complex formation by DCs in vivo. Histograms show MHCII-p on CD8$^+$DEC205$^+$ and CD8$^-$33D1$^+$ DCs 30 min, 3 hours, and 1 or 2 days after intravenous injection of 10 μg of αDEC205-HEL or 33D1-HEL or Iso-HEL control in (**A**) B10.BR and (**B**) C3H/He] mice. (**C**) Histograms show MHCII-p on CD8$^+$DEC205$^+$ and CD8$^-$33D1$^+$ DCs 30 min, 3 hours, and 1 day after intravenous injection of 30 μg of αhDEC205-HEL into CD11c-hDEC205 transgenic (hDEC$^+$) or control littermate (C57BL/6 × B10.BR) mice (hDEC$^-$). Arrows indicate significant staining as compared with controls.

and green fluorescent protein (GFP) (fig. S10A). Infected cells expressing the retrovirally encoded DCIR2 were then sorted on the basis of GFP expression and targeted with αDEC205-OVA or 33D1-OVA in vitro. Following DC maturation with LPS, presentation to OT-II T cells was equivalent for the two targeting antibodies [fig. S10B and (*13*)]. This shows that class II presentation by mature bone marrow–derived DCs (BMDCs) was independent of whether they were targeted by αDEC205-OVA or 33D1-OVA. We conclude that the difference in MHCII processing by DC subsets is an intrinsic property of the cell and not due to differences between the receptors targeted by αDEC205 or 33D1 mAbs.

Many of the proteins that regulate MHCI and MHCII processing pathways have been described and their expression documented in DCs (*19*, *20*). To determine whether the two DC subsets show systematic intrinsic differences in expression of components of the MHCI and MHCII processing machinery, we performed microarray experiments on mRNA isolated from the two DC subsets (Fig. 4, A and B; fig. S11A) (*13*). We found that the two DC subsets differentially express components of the MHCI and MHCII processing pathways in a manner consistent with their ability to produce MHCII-p and induce CD4 and CD8 T cell responses. CD8$^+$DEC205$^+$ DCs, which are biased for MHCI cross-presentation, were enriched in Tap1, Tap2, calreticulin, calnexin, Sec61, ERp57, ERAAP, as well as cystatin B and C, all of which are involved in MHCI presentation or inhibition of enzymes that process peptides for MHCII presentation (*19*, *20*) (Fig. 4B). In contrast, CD8$^-$33D1$^+$ DCs, which are biased for MHCII presentation, were enriched in cathepsins C, H, and Z, asparagine endopeptidase (AEP), GILT, and H2-Mbeta 1, all of which are implicated in the MHCII antigen processing pathway (*19*, *20*) (Fig. 4A). To confirm that these proteins were differentially expressed in DC subsets, we performed fluorescence-activated cell sorting (FACS) analysis for intracellular H2DM (Fig. 4C) and Western blotting experiments. MHCI processing–associated proteins were expressed at higher levels in CD8$^+$DEC205$^+$ DCs (Fig. 4E and fig. S11B), whereas MHCII processing proteins were expressed at higher levels in CD8$^-$33D1$^+$ DCs (Fig. 4, C to F, and fig. S11B). We conclude that the differences in expression of proteins involved in antigen processing in CD8$^+$DEC205$^+$ and CD8$^-$33D1$^+$ DCs are consistent with preferential processing of antigens for presentation by the two cell types.

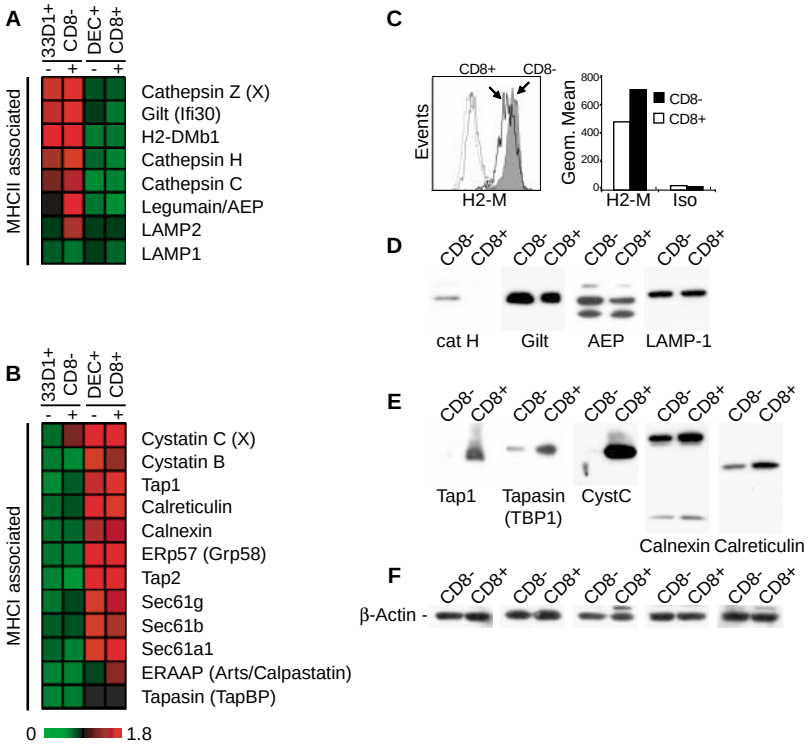

Fig. 4. Distinct expression pattern of MHC class I– and MHC class II–associated molecules. Affymetrix gene array analysis showing relative amounts of mRNAs associated with the MHC class II (**A**) and MHC class I (**B**) processing pathways expressed by CD8$^+$DEC205$^+$ and CD8$^-$33D1$^+$ DCs purified from WT- (–) and Flt3L-melanoma– (+) injected mice. Each bar represents the mean of three individual gene arrays prepared from distinct mRNA samples. (**C**) Intracellular FACS analysis of H2-DMb1/H2-DMa heterodimer in the CD8$^+$DEC205$^+$ and CD8$^-$33D1$^+$ DCs. (**D**) Western blots for cathepsin H, Gilt, and AEP on extracts of purified CD8$^+$DEC205$^+$ and CD8$^-$33D1$^+$ spleen DCs. (**E**) Western blots for Tap-1, tapasin, cystatin C, calnexin, and calreticulin on extracts of purified CD8$^+$DEC205$^+$ and CD8$^-$33D1$^+$ spleen DCs. (D) Lysosomal marker LAMP-1 (lysosomal-associated membrane protein 1) and (**F**) β-actin are shown as loading controls.

Efficient antigen presentation by DCs requires regulated lysosomal protein degradation (*21*, *22*). However, the requirements for presentation on MHCII and cross-presentation on MHCI differ in that MHCII processing occurs inside endosomes, whereas cross-presentation on MHCI necessitates antigen escape from the endosome into the cytoplasm to gain access to the proteasome and TAP transporters (*19*, *20*, *23*–*25*). Elegant in vitro experiments with cultured DCs show that during DC development, antigen presentation is regulated through control of lysosomal processing and MHCII cell surface transport (*21*, *22*, *26*–*28*). Cultured immature DCs capture antigen but only process and present it on MHCII after exposure to inflammatory stimuli or TLR ligation (*22*). This unique ability to sequester antigens may be important for their preservation during DC transit from sites of inflammation to lymphoid organs and might facilitate the escape of antigen from endosomes to the cytoplasm or endoplasmic reticulum for cross-presentation (*21*). However, DCs that fail to degrade antigen might also be suboptimal producers of MHCII-p. Our experiments show that in the intact host, this problem is resolved by producing a subset of DCs specialized for maximizing MHCII presentation. Although $CD8^{+}DEC205^{+}$ DCs can initiate immune responses by presenting on MHCII, $CD8^{-}33D1^{+}$ DCs excel in producing MHCII-p. This specialization may have important implications for understanding the initiation of T cell responses in vivo and for rational vaccine design.

References and Notes

1. Y. J. Liu, *Cell* **106**, 259 (2001).
2. K. Shortman, Y. J. Liu, *Nat. Rev. Immunol.* **2**, 151 (2002).
3. R. M. Steinman, D. Hawiger, M. C. Nussenzweig, *Annu. Rev. Immunol.* **21**, 685 (2003).
4. D. Vremec *et al.*, *J. Exp. Med.* **176**, 47 (1992).
5. M. D. Witmer, R. M. Steinman, *Am. J. Anat.* **170**, 465 (1984).
6. R. S. Allan *et al.*, *Science* **301**, 1925 (2003).
7. J. M. den Haan, S. M. Lehar, M. J. Bevan, *J. Exp. Med.* **192**, 1685 (2000).
8. T. Iyoda *et al.*, *J. Exp. Med.* **195**, 1289 (2002).
9. J. M. den Haan, M. J. Bevan, *J. Exp. Med.* **196**, 817 (2002).
10. J. L. Pooley, W. R. Heath, K. Shortman, *J. Immunol.* **166**, 5327 (2001).
11. C. Scheinecker, R. McHugh, E. M. Shevach, R. N. Germain, *J. Exp. Med.* **196**, 1079 (2002).
12. P. Schnorrer *et al.*, *Proc. Natl. Acad. Sci. U.S.A.* **103**, 10729 (2006).
13. Materials and methods are available as supporting material on *Science* Online.
14. D. Hawiger *et al.*, *J. Exp. Med.* **194**, 769 (2001).
15. M. C. Nussenzweig, R. M. Steinman, M. D. Witmer, B. Gutchinov, *Proc. Natl. Acad. Sci. U.S.A.* **79**, 161 (1982).
16. L. Bonifaz *et al.*, *J. Exp. Med.* **196**, 1627 (2002).
17. G. Dadaglio, C. A. Nelson, M. B. Deck, S. J. Petzold, E. R. Unanue, *Immunity* **6**, 727 (1997).
18. M. Guo *et al.*, *Hum. Immunol.* **61**, 729 (2000).
19. P. Bryant, H. Ploegh, *Curr. Opin. Immunol.* **16**, 96 (2004).
20. P. Cresswell, N. Bangia, T. Dick, G. Diedrich, *Immunol. Rev.* **172**, 21 (1999).
21. L. Delamarre, M. Pack, H. Chang, I. Mellman, E. S. Trombetta, *Science* **307**, 1630 (2005).
22. E. S. Trombetta, I. Mellman, *Annu. Rev. Immunol.* **23**, 975 (2005).
23. R. N. Germain, *Cell* **76**, 287 (1994).
24. N. Shastri, S. Cardinaud, S. R. Schwab, T. Serwold, J. Kunisawa, *Immunol. Rev.* **207**, 31 (2005).
25. J. W. Yewdell, C. C. Norbury, J. R. Bennink, *Adv. Immunol.* **73**, 1 (1999).
26. K. Inaba *et al.*, *J. Exp. Med.* **191**, 927 (2000).
27. P. Pierre, I. Mellman, *Cell* **93**, 1135 (1998).
28. S. J. Turley *et al.*, *Science* **288**, 522 (2000).

29. We thank K. Velinzon for cell sorting; K.-H. Yao for technical assistance; H.-K. Lee, S. H. Park, and S. Y. Joe for help generating CD11c-hDEC205 mice; A. Flores-Langarica, S. Boscardin, A. Gazumyan, E. Besmer, and F. Nimmerjahn for helpful discussion; the MSKCC Monoclonal Antibody Core Facility for labeling of antibodies; and MSKCC Genomics Core Laboratory for performing the microarrays. Supported by grants from the NIH (to C.G.P., R.M.S., and M.C.N.). D.D. is a fellow of the Deutsche Forschungsgemeinschaft (DU 548/1-1), and V.R.B. was supported by the German National Academic Foundation. M.C.N. is an Investigator with the Howard Hughes Medical Institute. M.C.N. and R.M.S. are on the scientific advisory board of Celldex, a startup company interested in targeting dendritic cells.

Supporting Online Material

www.sciencemag.org/cgi/content/full/315/5808/107/DC1
Materials and Methods
Figs. S1 to S11
References

10 October 2006; accepted 15 November 2006
10.1126/science.1136080

Differential Transmission of Actin Motion Within Focal Adhesions

Ke Hu,* Lin Ji,* Kathryn T. Applegate, Gaudenz Danuser,† Clare M. Waterman-Storer†

Cell migration requires the transmission of motion generated in the actin cytoskeleton to the extracellular environment through a complex assembly of proteins in focal adhesions. We developed correlational fluorescent speckle microscopy to measure the coupling of focal-adhesion proteins to actin filaments. Different classes of focal-adhesion structural and regulatory molecules exhibited varying degrees of correlated motions with actin filaments, indicating hierarchical transmission of actin motion through focal adhesions. Interactions between vinculin, talin, and actin filaments appear to constitute a slippage interface between the cytoskeleton and integrins, generating a molecular clutch that is regulated during the morphodynamic transitions of cell migration.

Directed cell migration involves spatiotemporal orchestration of protrusion at the leading cell edge, adhesion of the protrusion to the extracellular matrix (ECM), pulling against the adhesions to translocate the cell body, and weakening of the adhesion at the cell rear for advancement (*1*). In this process, actin filaments (F-actin) must couple to the ECM through the plasma membrane (*1*–*3*) via focal adhesions (FAs) to translate actin polymerization and/or actin-myosin contraction into cell motion. FAs are complexes of >100 different proteins linking F-actin to clustered transmembrane integrin ECM receptors (*2*, *4*). Regulating the attachment between F-actin and integrins via proteins within FAs is thought to be critical for controlling the spatiotemporal variability of protrusion and traction (*5*) and the ability of cells to respond to mechanical cues.

It is well established that F-actin and FAs are coupled to each other. Many FA proteins bind directly or indirectly to F-actin (*6*–*8*) and/or integrins (*9*–*13*). Contractile actomyosin bundles are often rooted in FAs (*2*, *4*), and perturbations of actomyosin cause changes in FAs and vice versa (*2*). Although the importance of spatiotemporal coordination between FAs and F-actin in cell migration is well appreciated (*2*, *14*, *15*), it is not known which FA molecules interact with F-actin in living cells, and the dynamics of molecules within these two assemblies have never been analyzed simultaneously. Predicting how FA proteins behave in vivo by biochemical data alone is impossible because of the complexity of their interactions (*4*).

To study the dynamic interactions between F-actin and FAs, we combined total internal reflection fluorescence microscopy (TIRFM) and fluorescent speckle microscopy (FSM). TIRFM optimizes image contrast at the ventral cell–ECM/coverslip interface where cortical F-actin integrates with FAs. FSM marks macromolecular assemblies with fluorophore clusters called speckles (fig. S1). Computational tracking of speckle motion allows mapping of protein dynamics with submicron resolution (*16*, *17*). We studied PtK1 cells migrating on coverslips, on which they organized a fibronectin-containing ECM (fig. S2).

To determine the spatial relations between FAs and F-actin flow, we captured image pairs using TIRFM of green fluorescent protein

Department of Cell Biology, The Scripps Research Institute, La Jolla, CA 92037, USA.

*These authors contributed equally to this work.
†To whom correspondence should be addressed. E-mail: waterman@scripps.edu (C.M.W.-S.); gdanuser@scripps.edu (G.D.)